Characteristic features of an active polar filament pushing a load

Prabhakar Maurya[1⋆], Shalabh K. Anand[1†] and Sunil P. Singh[1†⋆]

1 Department of Physics, Indian Institute Of Science Education and Research, Bhopal 462 066, Madhya Pradesh, India

⋆ mprabhakar537@gmail.com , † shalabh.kumar.anand@gmail.com , †⋆ spsingh@iiserb.ac.in

Abstract

We present the structural and dynamical behavior of an active polar filament, which is pushing loads of different magnitudes and sizes using overdamped Langevin dynamics simulations. By changing the bending rigidity and the connectivity between the filament and the load, we smoothly vary the filament's boundary conditions from pivoted to clamped. For the pivot boundary conditions, the active polar filament buckles and displays various fascinating dynamical phases: snake-like motion, rotational motion, bent shape conformations, and helical structures. However, in clamped boundary conditions, the helical phase disappears, and the filament attains either an extended state or a bent state. The transition from the extended-state conformation to the helical state is demarcated using the global helical order parameter in the parameter space of active force and a quantity associated with the boundary condition. We have obtained various power laws relating to the curvature radius of the helical phase, effective diffusivity, and rotational motion of the monomers with the active force. Additionally, we demonstrate that the filament's effective diffusivity in the helical phase shows a non-monotonic trend with the active force, increasing linearly followed by a sharp reduction at a high strength of the active force.

Received Date
Accepted Date
Published Date

Contents

1 Introduction **2**

2 Model **3**

3 Results **5**
3.1 Helical Transition 5
3.2 Bending Energy 6
3.3 Structural Properties 8
3.4 Bond Correlation 8
3.5 Dynamics 10
3.6 Size of the Load 11

4 Summary and Conclusion **12**

5 Acknowledgement 13

References 13

1 Introduction

Thin filamentous macromolecules play an indispensable role in the living matter [1–9], notably motility of the cells [10], movement of sperms [7, 8], bacterium [9, 11], transport of vesicles [12], muscle contraction [13], shape change in neurons, sensing and recasting of mechanical stresses into an electrical signal in vestibular sensing cells [14], division of cells [7, 8, 15, 16], etc. Such filaments experience mechanical forces, different from thermal origin, generated by various enzymes and motor proteins while performing biological functions. These stresses can induce substantial conformational changes [7–9]. Consequently, fascinating structural and dynamical phases emerge, *viz.* the beating and rotary motion of the cilia and flagellum, helical twisting of the chromosomes while replication [17–19], bending of stereocilia, beating and buckling of actin bundles, etc. With these insights, considerable progress has been made in unraveling the conformational dynamics of the active filaments in previous works [5, 8, 20, 21, 21, 22, 22–31].

Active polymers have been modeled predominantly via two distinct approaches, one assuming the active noise on the monomer exhibits the Ornstein-Uhlenbeck process [5, 21, 32–42], while the other one assumes the active process is quenched on the backbone of the polymer, imposing force along the polymer's conformational specifically unidirectionally along its every tangent-bond vector. The second category of active polymers are also referred as an active polar linear polymer (APLP) [8, 23, 43–47]. The former one leads to the non-monotonic behavior of the polymer [32, 41], while the latter model results in fascinating behavior with a coil-to-globule-like transition with a significant compression [23, 43, 44], for the case of the flexible polymer in the limit of large activity. A quite similar model has revealed a few aspects of very complex systems, such as the formation of chromatin compartments, enhanced segmental dynamics of chromatin, and macro-scale coherent motion of the chromatin [48–50]. On the other hand, a clamped active polar filament exhibits rotational and beating motion, and its structure [20, 22, 51, 52], is more like a rotating flagellum while freely moving, attains various structures such as strong bending, circular-shape and helical coiling [23, 44, 53].

The present work primarily assesses the variation of the boundary conditions of the load (front bead), the bending rigidity of the front bead with the rest of the filament (see Fig.1), the size of the monomer, and the strength of the compressive active force etc. These variations can result in novel configurations, especially the emergence of the dynamically stable helical state for the active polar filaments. Such helical structures are intriguing, as they appear in numerous biological functions; a few striking examples in living matter are listed here: the double-strand DNA, actin filaments, viral capsids [54], sub-units of proteins as α-helices [55], helical organization of bacterial chromosomes [17–19], etc. A long straight filament can acquire a helical buckled state under compressive flow or in a viscosity gradient [56, 57]. Understanding the kinetics and thermodynamic stability of the helices is crucial, and it can provide valuable insights into various biological functions.

This article presents a minimal model for the active polar filament in three dimensions (3D) with the active force imposed onto its backbone, which offers the appearance of dynamical structures and avoids self-trapping into the spiral form at two dimensions [8, 23, 58]. The sensitivity of the structural dynamics on the boundary conditions of the front monomer

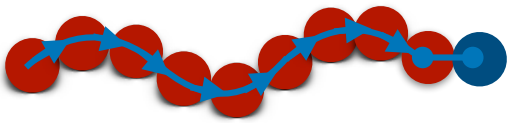

Figure 1: A schematic of an active filament with a load. Arrows indicate the direction of the active forces on monomers. The front monomer (blue) and its connection are shown differently. The connectivity of the front monomer with filament depicts that it can rotate depending on the boundary conditions.

and its load has already been pointed out in the case of polar semi-flexible and flexible polymers [20, 44, 59]. Using computer simulations, we comprehensively study an active filament under compressive force. A smaller bending rigidity (more flexibility) of the load with filament provides a higher drag. We observe a monotonic shrinkage of the filament with active force. A stable helical structure of the filament spontaneously emerges at a higher load and sufficiently high active force. This structure is stable up to a certain bending rigidity, which disappears at a higher bending connection (smaller load).

We demarcate structural transition using various physical parameters such as tangent-tangent correlation function, bending energy, and global helical order parameter (H_4). The correlation exhibits oscillatory behavior, and the helical order parameter also displays the monotonic transition from the extended state to the helical phase. Moreover, the curvature radius of the twist decreases with the activity. Further, we also analyzed the dynamical behavior of the filament using mean-squared displacement (MSD) and computed the self-diffusion coefficient of the filament. Strikingly, the effective diffusion coefficient of the active filament shows a non-monotonic behavior with the Péclet number. Surprisingly, for very large Péclet numbers, the effective diffusivity of the active filaments abruptly drops, and it nearly attains the passive limit. More importantly, the internal dynamics of the monomers reveal that in the helical phase, the motion of monomers is oscillatory, where they rotate along the axis of the helix, and the rotation frequency grows with a power-law on Péclet number given as $Pe^{7/4}$. The oscillation frequency's power-law variation is described using a straightforward scaling relation in terms of the curvature radius.

The manuscript is organized as follows: the model of the active filament and its description of the load and parameters are provided in the Model Section. The structural transition of the filament, helical order parameter, and dynamical quantities are identified and discussed in the Results Section. Furthermore, we summarise our study in the Conclusion Section.

2 Model

We model an active filament as a linear polymer of N spherical Brownian monomers linearly connected through harmonic springs. These monomers interact among themselves via excluded volume interactions. In addition, the bending potential to control the stiffness of the backbone of the filament is also incorporated. Thus, the total energy of the filament can be written as $U = U_s + U_b + U_{LJ}$. Here, U_s, U_b, and U_{LJ} are spring, bending, and excluded volume potentials, respectively. The spring potential U_s of the filament is written as

$$U_s = \frac{k_s}{2} \sum_{i=1}^{N-1} (|\boldsymbol{r}_{i+1} - \boldsymbol{r}_i| - \ell_0)^2, \tag{1}$$

where k_s and ℓ_0 are the spring constant and the equilibrium bond length, respectively, and $\boldsymbol{r}_i$ is the position vector of the i^{th} monomer.

The bending potential U_b provides stiffness to the backbone of the filament is given as

$$U_b = \frac{\kappa_B}{2}\sum_{i=1}^{N-2}(\boldsymbol{R}_{i-1} - \boldsymbol{R}_i)^2. \tag{2}$$

Here $\boldsymbol{R}_i$ is i^{th} bond vector, $\boldsymbol{R}_i = \boldsymbol{r}_{i+1} - \boldsymbol{r}_i$ and κ_B is the bending rigidity of the filament. The stiffness of a filament is defined in terms of persistence length ℓ_p which can be expressed in terms of κ_B as $\ell_p = \kappa_B \ell_0^3/(k_B T)$, with $k_B T$ being thermal energy.

The excluded volume potential, U_{LJ}, is implemented via the repulsive part of the Lennard-Jones potential. More specifically, for a distance $R_{ij} < 2^{1/6}\sigma$ between two monomers i and j

$$U_{LJ} = \sum_{i>j}^{N} 4\epsilon\left[\left(\frac{\sigma}{R_{ij}}\right)^{12} - \left(\frac{\sigma}{R_{ij}}\right)^{6} + \frac{1}{4}\right], \tag{3}$$

and $U_{LJ} = 0$ for $R_{ij} \geq 2^{1/6}\sigma$. Here, σ and ϵ are the LJ diameter of a monomer and the LJ interaction energy between monomers, respectively.

The dynamics of the active filament is governed by the over-damped Langevin equation

$$\gamma_i \dot{\boldsymbol{r}}_i(t) = -\nabla_i U + \boldsymbol{F}_a^i(t) + \boldsymbol{F}_t^i(t). \tag{4}$$

Here γ_i is the viscous drag coefficient, $\boldsymbol{F}_a^i$ is the active force, and $\boldsymbol{F}_t^i$ is the thermal noise with zero mean. The second moment of the thermal noise obeys the fluctuation-dissipation relation (FDT)

$$\langle \boldsymbol{F}_t^i(t) \cdot \boldsymbol{F}_t^j(t')\rangle = 6k_B T\gamma_i \delta_{ij}\delta(t-t'). \tag{5}$$

The active force acts along the bond direction, for the i^{th} bond vector is given as $f_a \boldsymbol{R}_i/|\boldsymbol{R}_i| = f_a \hat{\boldsymbol{t}}_i$, where $\hat{\boldsymbol{t}}_i$ is the i^{th} unit bond vector and f_a is magnitude of active force. Thus, active force on i^{th} monomer, presented as $\boldsymbol{F}_a^i$ in Eq. 4, has contributions shared by i^{th} and $(i-1)^{th}$ bonds. This can be expressed by adding contribution from both bonds, which yields $\boldsymbol{F}_a^i = \frac{1}{2} f_a(\hat{\boldsymbol{t}}_i + \hat{\boldsymbol{t}}_{i-1})$. The strength of the active force on a monomer can be expressed in terms of a dimensionless number called Péclet number, which is defined as the ratio of the active force with thermal energy, $Pe = f_a \ell_0/(k_B T)$.

Additionally, the front monomer is considered different from other monomers of the filament, therefore the front monomer's bending rigidity (κ_B^h), the size (σ^h), and friction coefficient (γ_t^h) are taken independent parameters. In the case of the polar filament, the front/head monomer acts as a load. Alignment of the load with the rest of the filament can be tuned by changing the bending stiffness (κ_B^h) of the bond connected to the front-most monomer; random alignment of the head from the rest of the filament acts higher load to the filament, therefore by tuning the bending (κ_B^h) we can change the strength of the load. This is measured in terms of the ratio of the dimensionless parameter $\rho = \kappa_B^h/\kappa_B$ as the control parameter that changes the boundary condition through which the load is attached to the front of the filament. The boundary condition from pivot ($\rho = 0$) to clamped ($\rho = 1$) is varied by ρ. For $\rho = 0$, it allows the load to freely rotate from the filament's axis, whereas the fluctuations out of the axis are suppressed for $\rho \geq 1$. The model restores to the tangentially propelled filament for the case of $\rho = 1$, except for the front bead, which does not experience the active force.

Aside from changing the stiffness of the load, the size of the load, $\alpha = \sigma^h/\sigma$, is also varied while keeping the bending stiffness same as the rest of filament, i.e., $\kappa_B^h = \kappa_B$. Here, α is the control parameter, which varies the diameter of the load, while doing so, we make sure that the equilibrium bond length corresponding to the load also changes as follows: $\ell_0^h = 0.5(\sigma + \sigma^h)$. The results corresponding to this aspect are discussed at the end of the manuscript.

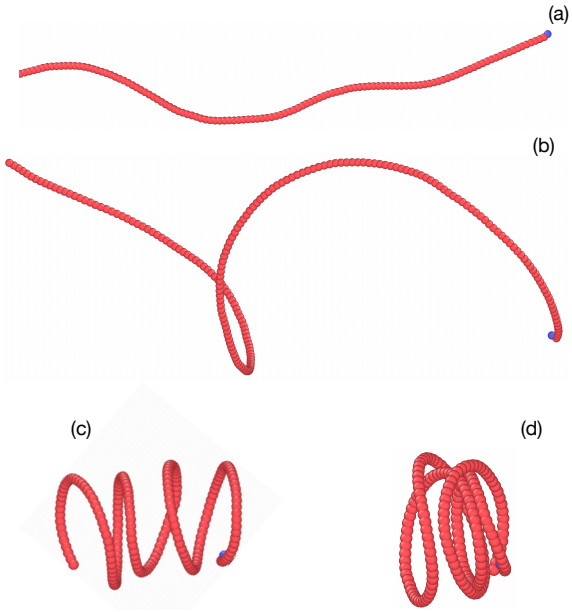

Figure 2: Various snapshots of the active polar filament for (a) $Pe = 10$, (b) $Pe = 40$, and (c) and (d) $Pe = 160$ at, for $\rho = 0$. Notably, the front monomer is presented in red color.

All the physical parameters in this manuscript are scaled in the units of the bond length ℓ_0, the diffusion coefficient of a monomer D_0, and thermal energy k_BT. Simulations parameters are chosen as $k_s = 1000 k_BT/\ell_0^2, \sigma = \ell_0, \epsilon/(k_BT) = 10$, time is in units of $\tau = \ell_0^2/D_0$, and the stiffness parameter κ_B is in units of k_BT/ℓ_0^2 and is fixed to be 1000 unless otherwise mentioned. All the simulations are performed in a three-dimensional space. The Euler integration method is used with a time-step in the range of $10^{-4}\tau$ to $10^{-5}\tau$ throughout to ensure the stability of the simulation. For good statistics, each data set is averaged over at least ten independent runs for all the results presented in this manuscript.

3 Results

We first investigate the structural behavior of a tangentially driven active polar filament, focusing on the head monomer, which serves as a load, by systematically varying its connection to the filament as well as its friction and size. We analyze how these changes affect the filament's conformation and dynamics. The boundary condition between the head and the filament is controlled by the bending rigidity (κ_B^h) of the bond connecting the load, which differs from the bending rigidity of the other bonds (κ_B). We express this difference as a ratio of the bending parameters defined $\rho = \kappa_B^h/\kappa_B$. For $\rho = 0$, the bond acts as a pivot between load and filament, allowing the head monomer to rotate freely relative to the rest of the filament; we refer to this as the pivot boundary condition. Conversely, when $\rho \geq 1$, the load is tightly coupled to the filament's orientation, which will be called as the clamped boundary condition.

3.1 Helical Transition

A long, straight filament under a compressive active force tends to buckle, which can result in either correlated buckling or uncorrelated folding of the filament [44]. We observe that the filament transitions through various structures, from rod-like to helical conformations, as

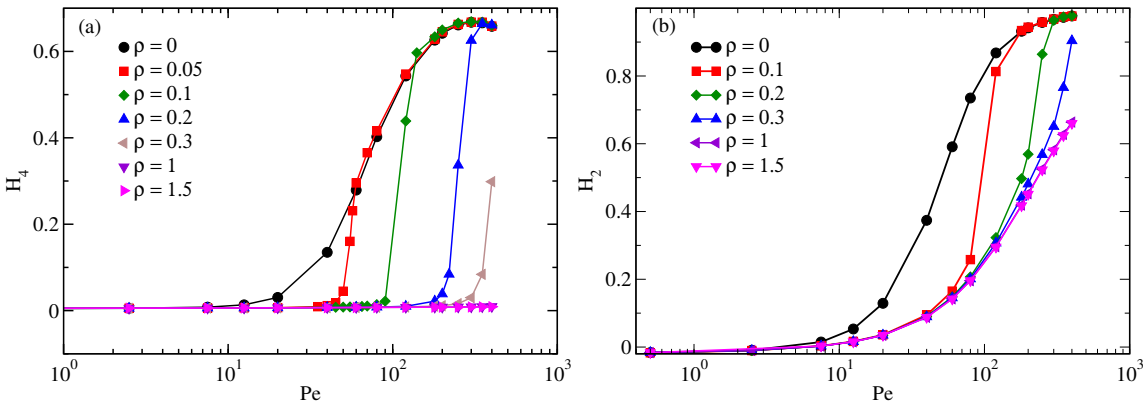

Figure 3: a) Average global helical order parameter H_4 as a function of Pe for different ρ. b) The variation of the local order parameter H_2 as a function of Pe for various ρ as indicated in the legend.

illustrated in Fig. 2. We calculate the helical order parameters to quantify structural transitions. For this we follow the approach of Ref. [60–62] to compute the global (H_4) and local (H_2) helical order parameters

$$\begin{aligned} H_4 &= \left(\frac{1}{N-2}\sum_{i=1}^{N-1}\hat{\mathbf{t}}_i\right)^2, \\ H_2 &= \frac{1}{N-3}\sum_{i=2}^{N-2}\hat{\mathbf{t}}_i\cdot\hat{\mathbf{t}}_{i+1}. \end{aligned} \tag{6}$$

The H_4 measures the global twist of the filament; conversely, H_2 characterizes the local twist of the filament.

The computed values of H_4 are presented in Fig. 3-(a) for various ρ as a function of P'eclet number (Pe). For $\rho \leq 1$, $H_4 \approx 0$ suggests that the filament does not exhibit a global twist. If the bending rigidity of the filament with the load is the same or greater, the polar filament does not support global buckling. Furthermore, as ρ decreases, there is a sharp increase in the values of H_4. As shown in the plot, H_4 suddenly rises from zero to a large value as Pe increases. In the limit of large Pe, H_4 nearly saturates to a common value for all $\rho < 0.3$. The appearance of non-zero values in H_4 indicates a transition point for a given ρ. It is also interesting to note that for larger values of $\rho \geq 1$, the filament does exhibit local bending despite its $H_4 \approx 0$, the local bending can be measured in terms of H_2 which increases with Pe, as shown in Fig. 3-(b). Despite the local bending, the filament does not attain the helical shape and global order parameter $H_4 \approx 0$. Moreover, for $\rho < 1$, H_2 also sharply rises and reaches a common plateau value for all ρ. The difference between H_4 and H_2 is that in the extended phase, $H_4 \approx 0$ while H_2 is non-zero and grows with Pe for all ρ, see Fig. 3-(b).

3.2 Bending Energy

The helical buckling of the filament is achieved under compressive force, which exhibits higher bending energy than a linearly extended filament. The structural transition of the filament can also be marked by the bending energy of the filament. For this, we present the average bending energy U_b of the filament in Fig. 4 as a function of Pe for various values of ρ.

The bending energy remains unchanged for small Péclet numbers $Pe < 10$, for the range of ρ covered. Beyond $Pe > 10$, a systematic monotonic increase in the bending energy appears as Fig. 4 displays for $\rho = 0$. For $\rho > 0$ values, the plateau range extends beyond $Pe > 10$.

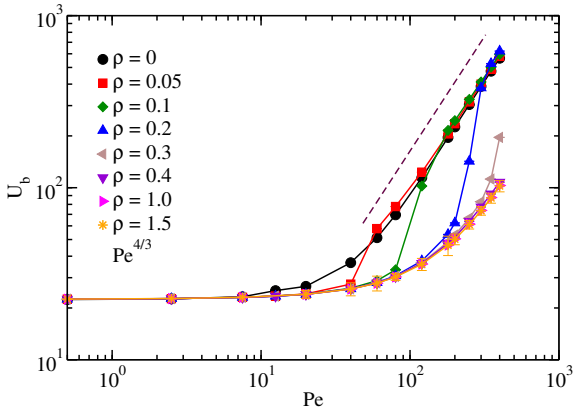

Figure 4: The variation of the bending energy (U_b) as a function of Pe for various ρ as indicated in the legend. The dashed line illustrates the power law behavior of the bending energy ($U_b \sim Pe^{4/3}$) with an exponent 4/3 in the helical phase.

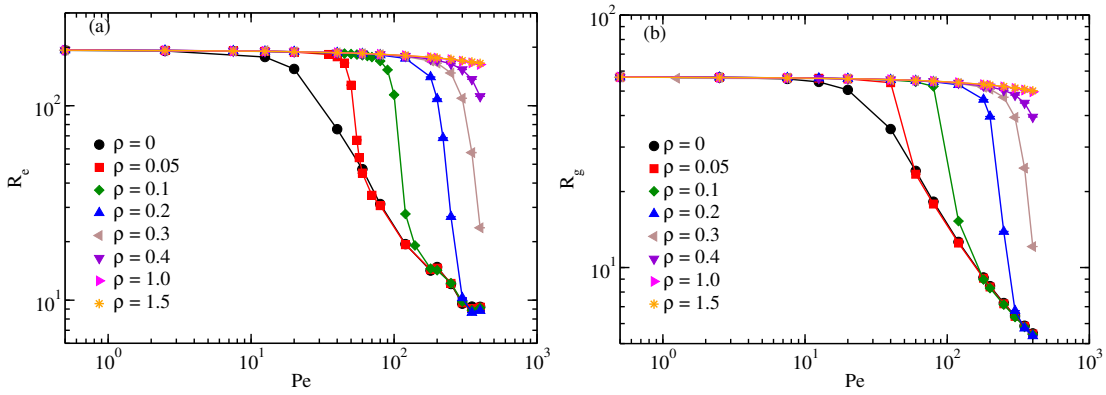

Figure 5: a) The variation of the average end-to-end distance R_e as a function of the Péclet number Pe. b) The average radius of gyration R_g of the filament as a function of Péclet number Pe for various ρ as displayed in the plot.

Importantly, a sharp transition in bending energy is observed at a critical Péclet number for $\rho > 0$. At this juncture, bending energy curves merge on the behavior of $\rho = 0$. A sharp upsurge in the bending energy for $\rho < 1$ at the critical Péclet number indicates that the filament undergoes structural transition from the extended-state to a more curved state, in this case, a helical state, as Fig. 3-(a) also displays the spontaneous emergence of non-zero values of H_4. It's important to emphasize here that the transition from the extended state to the helical state for the $\rho = 0$ is gradual rather than sudden as for $\rho > 0$. The bending energy in the helical phase displays a power law variation with $U_b \sim Pe^{4/3}$, as a dashed line illustrates this variation for $Pe > 10$.

The transition point, where an upsurge in the bending energy is observed, shifts towards higher Pe with an increase in ρ. Notably, we observe two universal bending energy curves, one corresponding to the helical shape and the other one corresponding to the extended-state or folded conformations. A change in the bending rigidity of the load oversees the transition from lower bending energy to higher bending energy state. This reveals that despite higher bending energy, the helical state appears to be more stable conformations under compressive active force; these conformations are stabilized by the compensation of compressive force with the viscous drag.

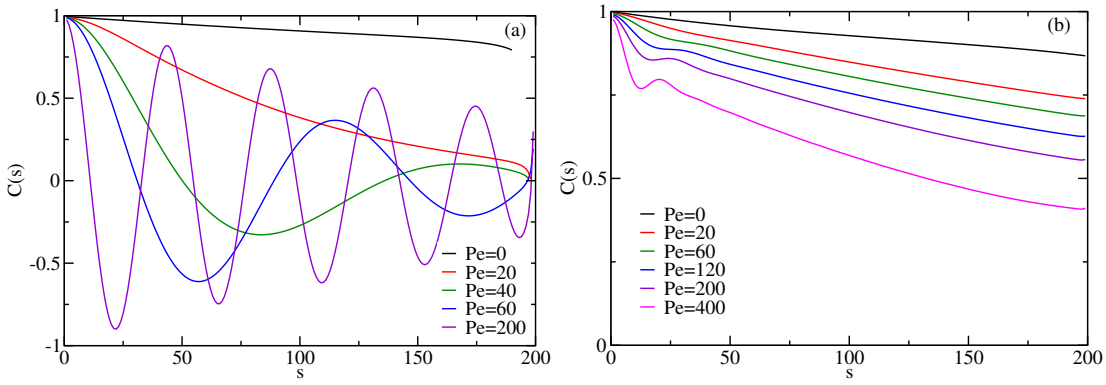

Figure 6: Tangent-tangent correlation ($C(s)$) of the active polar filament for different Pe strengths at a) $\rho = 0$ and b) $\rho = 1$, here, $s = 0$ and $s = N$ corresponds to tail and head monomers of the filament, respectively.

3.3 Structural Properties

We illustrate the change in the structure of active polar filament using average end-to-end distance (R_e) and radius of gyration (R_g) read as

$$\begin{aligned} R_e &= \langle\sqrt{(\boldsymbol{r}_1 - \boldsymbol{r}_N)^2}\rangle, \\ R_g &= \left\langle\sqrt{\frac{1}{N}\sum_{i=1}^{N}(\boldsymbol{r}_i - \boldsymbol{r}_{cm})^2}\right\rangle. \end{aligned} \tag{7}$$

Here, $\boldsymbol{r}_{cm}$ is the center of mass of the filament, and angular brackets represent the ensemble average. Figure 5 displays the computed values of R_e and R_g on the parameter space of Pe and ρ.

For the pivot boundary conditions $\rho = 0$, as expected, conformations are nearly unperturbed for the small activity $Pe < 10$; therefore, R_e and R_g remain unchanged. However, beyond a critical $Pe > 10$, R_e and R_g monotonically decrease, see Fig. 5 (a) and (b), respectively. The filament is substantially compressed for larger values of Pe, as R_g and R_e show a significant reduction from its equilibrium value in the presented Pe range.

Furthermore, an increase in the ρ yields the crossover from a plateau to compression of R_e and R_g for larger values of Pe. Importantly, the compression of the filament appears abrupt in nature, as also seen in the sharp variation of the bending energy and helical order parameter. For sufficiently large Pe, it merges with the behavior of the $\rho = 0$. In the limit of the clamped boundary condition $\rho \geq 1$, where the head/load is connected rigidly with the filament, the structure of the active filament is nearly unchanged in the presented simulation window, indicating that the filament remains in the extended state. Therefore, no structural transition is observed here. In the limit $\rho > 1$, the active force can lead to bending without helical phase; thereby, compression is observed [8, 44].

3.4 Bond Correlation

The monotonic compaction of R_e and R_g and the helical order parameter indicate that the filament acquires folded/buckled conformations and exhibits fascinating structural transitions as snapshots and supporting media files (see Movie 1, 2, and 3) to corroborate our claim.

We look into spatial correlation along the contour to compute the curvature of the filament. For this, tangent-tangent correlation is a useful metric. The correlation at separations of arc length $s = |i - j|\ell_0$ can be computed as $C(s) =< \hat{\boldsymbol{t}}_i.\hat{\boldsymbol{t}}_j >$. Specifically, the correlation

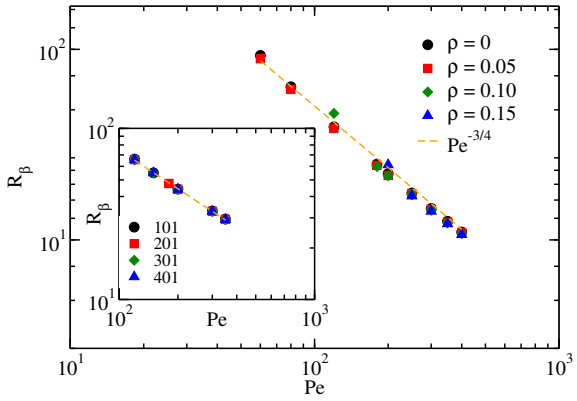

Figure 7: Radius of curvature (R_β) of the filament obtained from Eq. 8 as a function of the Péclet number Pe for various values of ρ. The dashed line shows the power law behavior of the curvature radius $R_\beta \sim Pe^{-\beta}$ with an exponent $\beta = 3/4$. Inset displays the curvature radius R_β as a function of Pe for various chain lengths at $\rho = 0$.

is computed from the rear end of the filament towards the front load, i.e., from $i = 1,...N$, and N is the load/head monomer. In equilibrium, the tangent correlation exponentially diminishes, providing the filament's persistence length ℓ_p, as correlation obeys exponential behavior, $C(s) \sim \exp(-s/\ell_p)$. The exponential behavior is nicely captured in Fig. 6 for $Pe = 0$, particularly for those Pe below the critical Pe for all ρ [41].

The tangential correlation diminishes substantially upon augment of Péclet numbers, indicating the lateral fluctuations along the contour are increased [44]. Interestingly, for $Pe \geq 40$, an exponential to damped oscillatory correlation behavior emerges. The oscillation in $C(s)$ becomes more prominent for large Pe and continues along its backbone. The transition from exponential behavior to sinusoidal oscillations with Pe is a signature of the underlying helical folding of the filament [44, 63].

For the stiffer boundary conditions (clamped), i.e., $\rho \geq 1$, Fig. 6-(b) illustrates that the sinusoidal oscillation in the correlation is absent, even in the limit of very high Péclet numbers $Pe > 100$. Rather, a two-step decay in the correlation function with a kink, which becomes more prominent for larger Pe and shifts towards the tail, i.e., smaller values of s. This implies that the filament attains a sharp fold, more like a hairpin. Seemingly, a similar behavior for the flexible active polar polymers has been observed, where tangent-tangent correlation exhibits negative correlation or the polymer is relatively more compressed near the head-side than the tail-side [34, 46, 47].

The oscillatory behavior of correlation can provide an approximate measure of the curvature radius of the filament. To estimate this, we examine the behavior of tangent-tangent correlations by fitting a damped oscillatory function using the following function,

$$C(s) = a_\beta \exp(-s/\ell_p)\cos(2\pi s/R_\beta). \tag{8}$$

Here, a_β is a constant, ℓ_p is the persistence length of the filament, and R_β is the characteristic length scale associated with the radius of curvature of the filament in the helical phase. Figure 7 displays the curvature-radius (R_β) obtained by fitting above Eq. 8 to the correlation function $C(s)$. The obtained curvature radius decreases with activity; more importantly, it follows a power law behavior, with a universal curve for all ρ as Fig. 7 displays a superimposed curve for all ρ. The obtained curvature radius exhibits a power law behavior $R_\beta \sim Pe^{-\beta}$ with an exponent $\beta \approx 3/4$. This characteristic feature of the curvature radius is also consistent for larger lengths, as illustrated in the inset of Fig. 7. The curvature radius is independent of the polymer length; a similar feature has also been reported for the passive filament under

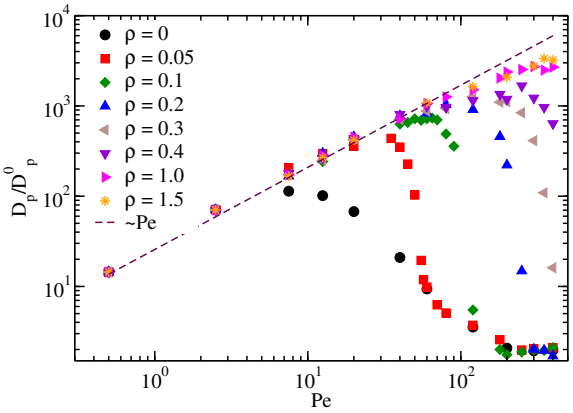

Figure 8: The scaled effective diffusion coefficient (D_p/D_p^0) as a function of Pe for various ρ. The dashed line indicates the linear behavior of scaled effective diffusivity D_p/D_p^0 as a function of Pe.

compressive flow [56].

3.5 Dynamics

The dynamics of an active filament is characterized by mean-squared displacement (MSD) of the center of the mass. In addition, insight into the internal dynamics can also be gained by probing monomers' MSD. First, we compute the MSD of the center of mass of the filament given as $< \Delta \boldsymbol{r}_{cm}^2(t) > = < [\boldsymbol{r}_{cm}(t) - \boldsymbol{r}_{cm}(0)]^2 >$, here angular bracket stands for the ensemble average. The MSD of an active filament exhibits a ballistic regime in a short time scale, $< \Delta \boldsymbol{r}_{cm}^2(t) > \sim t^2$, is superseded by the diffusive linear regime, $< \Delta \boldsymbol{r}_{cm}^2(t) > = 6D_p t$ at long time scales.

Figure 8 displays the filament's effective diffusivity (D_p) scaled with the diffusivity of the passive filament (D_p^0) estimated from the linear regime of the MSD. The effective diffusion coefficient, as expected, grows linearly with Pe, in the extended state of the filament for $\rho \geq 1$. This linear behavior of the effective diffusivity has been addressed for the case of active polar linear polymer (APLP) in the simulations and theory [43–45]. Here, the effective diffusivity can be expressed in the following form, $D_p = D_p^0(1 + a_\rho Pe)$, where D_p^0 is the diffusivity of the filament in the passive limit, and a_ρ is some model dependent constant.

For $\rho < 1$, the diffusivity also grows linearly, superimposing with the curves of $\rho \geq 1$. Aside from that, beyond a critical Pe, it deviates from the linear regime, followed by a sharp descent with Pe. Furthermore, in the limit of large $Pe > 200$ and $\rho < 0.3$, effective diffusivity reaches to the plateau value which is very close to the passive limit, as Fig. 8-(b) depicts. The decrease in the D_p is due to the helical buckling of the filament, where the active force acts along the curved conformations. This suppresses the large-scale directed motion of the filament. Hence, effective diffusivity is substantially suppressed compared to those for the elongated conformations. Thus, the helical shape polar filament diffuses much more slowly than the extended state filament.

We analyze the internal dynamics of the filament using the MSD of monomers in the considered parameter regime. Figure 9 displays the MSD of the front monomer in the center-of-mass reference frame. As expected, the MSD of the monomer grows superdiffusively before approaching the plateau for all Pe. The plateau regime of the MSD indicates that the monomers can not diffuse beyond the scale of filament length.

Markedly, in the intermediate Pe regime, MSD demonstrates an oscillatory behavior just before approaching the saturation limit. This intriguing oscillatory component of the MSD ap-

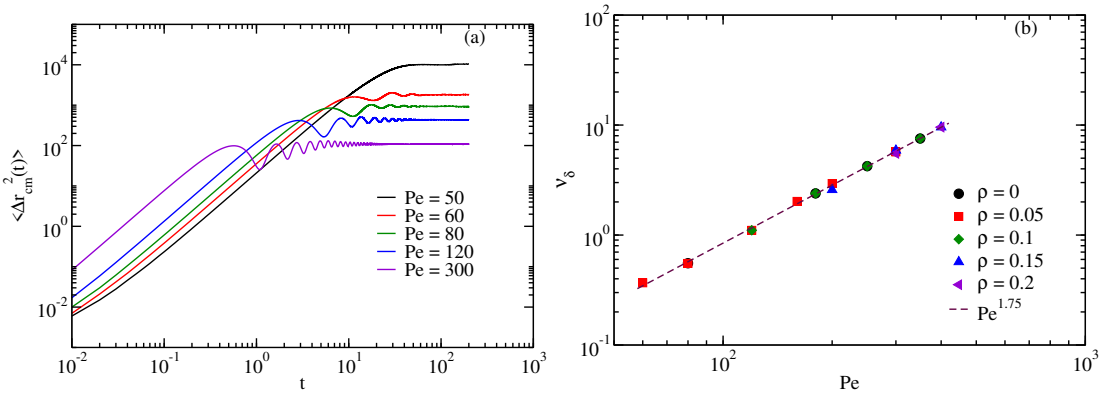

Figure 9: a) Mean-squared-displacement (MSD) of the end monomer with respect to the center of mass of the filament for various Pe at a given $\rho = 0.05$. b) The rotation frequency computed from oscillations of MSD of the monomers for various ρ. The dashed line displays the power variation of the frequency $\nu_\delta \sim Pe^{7/4}$.

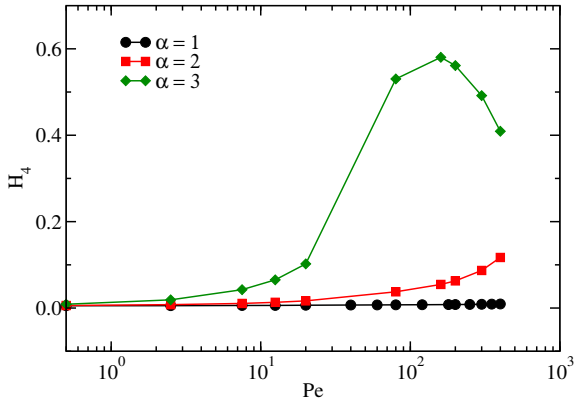

Figure 10: The global helical order parameter H_4 as a function of Pe at $\rho = 1$ for various load size $\alpha = 1, 2$, and 3.

pears in the helical phase, indicating the monomers are undergoing rotational motion around the axis of the helical conformations. Thereby, the filament also rotates clockwise/anticlockwise with a similar frequency. The rotational motion becomes more prominent for larger Péclet numbers with larger values of oscillation frequency. The rotational motion of the monomer is illustrated in the supporting movie-3.

Figure 9-(b) presents the oscillation frequency (ν_δ) of the monomer in the helical phase. The frequency ν_δ increases with Péclet number with a power law given as $\nu_\delta \sim Pe^\delta$, with an exponent $\delta \approx 7/4$. More importantly, ν_δ is independent of ρ likewise R_β. The oscillation frequency can be described by the following scaling arguments: the speed v_m of a monomer in the helical phase can be expressed as $v_m \approx R_\beta \nu_\delta$, where R_β is curvature radius. Employing the scaling relation of R_β obtained in Fig. 7 and assuming the speed of the monomer grows linear in Péclet number $v_m \sim Pe$, we can express $\nu_\delta \approx Pe/R_\beta$. Further, this can be expressed using the scaling relation obtained for the curvature radius as $\nu_\delta \approx Pe^{7/4}$, which reveals a similar exponent as in simulations, see Fig.9-(b).

3.6 Size of the Load

Now, we vary the size of the load while keeping κ_B^h same as κ_B, so we keep $\rho = 1$ in our simulations. Figure 10 compares the filament's mean helical order parameter H_4 with Pe for

three different sizes of loads as mentioned in Fig. 10. For the diameter $\sigma^h/\sigma = 1$, the filament is the same as presented in Fig. 3-(a) for $\rho = 1$. In this case, we observe no helix formation, thus a helical order parameter with nearly zero value of H_4. For the load size of $\sigma^h/\sigma = 2$ and $\sigma^h/\sigma = 3$, respectively. We observe a similar trend of H_4 with Pe as we presented earlier for the smaller values of $\rho < 1$. This indicates that the filament transitions to a helical structure as the load size increases. Our analysis of the diffusion coefficient and radius of gyration supports this observation, showing comparable trends to those discussed previously. Thus, the behavior of the active polar filament with a larger load is nearly analogous to that of a filament with a pivot boundary condition.

4 Summary and Conclusion

We have presented the conformational and dynamical features of an active polar filament pushing against a load. Different emergent phases of the filament are attained by systematically varying the size of the load or by tuning the filament's connectivity to the load. Our findings reveal an intriguing structural transition; under sufficiently high active forces, the filament adopts helical conformations despite the absence of torsional rigidity. These helical structures emerge as stable conformations despite having a higher bending energy than the extended state. The helical phase emerges in the broad regime of Péclet number and the bending parameter (ρ) of load. The transition from extended to helical conformations is marked by non-zero values of the global helical order parameter (H_4) and a sharp rise in the filament's bending energy. Compressive load induces helical buckling, even though this results in higher bending energy due to the combined effects of active force and viscous drag [44, 63].

In this study, we have modeled the load by changing the boundary condition slightly at the microscopic level, which has led to a large-scale macroscopic influence on the filament's structure and dynamics. A smaller variation of the load's bending rigidity allows more rotational freedom. Hence, the load is less aligned with the filament; therefore, this acts as an effectively higher drag/load on the filament against the compressive force, resulting in helical buckling. As the bending stiffness at the front is raised, the fluctuations in the bond orientations of the first monomer are substantially suppressed, and rotation of the front monomer is penalized; thus, the helical structure disappears in this parameter regime. At $\rho \geq 1$, larger bending stiffness at the front bead aligns with the filament; therefore, we do not witness a significant change in the structure.

Furthermore, we determined the curvature radius of the filament in the helical phase that decreased with compressive active force. The behavior of curvature radius is characterized by a power law $R_\beta \sim Pe^{-\beta}$ where $\beta \approx 3/4$. Furthermore, the filament displays fascinating dynamical behavior, too. Strikingly, the effective diffusion coefficient of the active filament shows a non-monotonic behavior with the Péclet number. Surprisingly, for very large Péclet numbers, the diffusivity of the active filaments abruptly drops to very small values, nearly attaining the passive limit despite a very large active force. A closer analysis of the internal dynamics revealed that monomers are undergoing oscillatory motion into the helical phase around its axis, which causes a sharp drop in the effective diffusivity. The rotational frequency corresponding to that is described by a power-law on Péclet number given as $\nu_\delta \sim Pe^{7/4}$.

Additionally, we have looked into the effect of the variation in size while maintaining the boundary condition. In this scenario, the filament also displays the transition from the extended state to the helical phase due to higher drag. Thus, a larger drag on the load, either by the random orientation due to a change in boundary condition or a bigger load size, results in the large-scale macroscopic structural and dynamical transition of the active filament. In summary, the manuscript highlights how the structural and dynamic behavior of the active

filament can be controlled by attaching a load with tunable size or connectivity. Such findings provide valuable insights into both natural microswimmers and artificial swimmers pushing a load [7, 8, 64]. The solvent-mediated hydrodynamic interactions among the monomers can open up many more interesting questions and provide more valuable insights into such systems [7, 8, 37].

5 Acknowledgement

The computational facilities at IISER Bhopal are highly acknowledged for providing computational time.

Funding information SPS and PM acknowledge financial support from the DST-SERB Grant No. CRG/2020/000661.

References

[1] J. Howard and R. Clark, *Mechanics of motor proteins and the cytoskeleton*, Appl. Mech. Rev. **55**(2), B39 (2002).

[2] Y. Harada, A. Noguchi, A. Kishino and T. Yanagida, *Sliding movement of single actin filaments on one-headed myosin filaments*, Nature **326**(6115), 805 (1987).

[3] F. Ndlec, T. Surrey, A. C. Maggs and S. Leibler, *Self-organization of microtubules and motors*, Nature **389**(6648), 305 (1997).

[4] T. Heeremans, A. Deblais, D. Bonn and S. Woutersen, *Chromatographic separation of active polymer–like worm mixtures by contour length and activity*, Science Advances **8**(23), eabj7918 (2022).

[5] R. G. Winkler, J. Elgeti and G. Gompper, *Active polymers—emergent conformational and dynamical properties: A brief review*, Journal of the Physical Society of Japan **86**(10), 101014 (2017).

[6] R. K. Manna and P. S. Kumar, *Emergent topological phenomena in active polymeric fluids*, Soft Matter **15**(3), 477 (2019).

[7] M. C. Marchetti, J.-F. Joanny, S. Ramaswamy, T. B. Liverpool, J. Prost, M. Rao and R. A. Simha, *Hydrodynamics of soft active matter*, Reviews of modern physics **85**(3), 1143 (2013).

[8] J. Elgeti, R. G. Winkler and G. Gompper, *Physics of microswimmers—single particle motion and collective behavior: a review*, Reports on progress in physics **78**(5), 056601 (2015).

[9] C. Bechinger, R. Di Leonardo, H. Löwen, C. Reichhardt, G. Volpe and G. Volpe, *Active particles in complex and crowded environments*, Reviews of Modern Physics **88**(4), 045006 (2016).

[10] K. M. Yamada and M. Sixt, *Mechanisms of 3d cell migration*, Nature Reviews Molecular Cell Biology **20**(12), 738 (2019), doi:10.1038/s41580-019-0172-9.

[11] H. C. Berg, *The rotary motor of bacterial flagella*, Annual review of biochemistry **72**(1), 19 (2003).

[12] W. W. Ahmed and T. A. Saif, *Active transport of vesicles in neurons is modulated by mechanical tension*, Scientific reports **4**(1), 4481 (2014).

[13] G. H. Koenderink, Z. Dogic, F. Nakamura, P. M. Bendix, F. C. MacKintosh, J. H. Hartwig, T. P. Stossel and D. A. Weitz, *An active biopolymer network controlled by molecular motors*, Proceedings of the National Academy of Sciences **106**(36), 15192 (2009).

[14] D. E. Angelaki and K. E. Cullen, *Vestibular system: the many facets of a multimodal sense*, Annu. Rev. Neurosci. **31**(1), 125 (2008).

[15] D. Mazia, *Mitosis and the physiology of cell division*, In *The cell*, pp. 77–412. Elsevier (1961).

[16] J. M. Scholey, I. Brust-Mascher and A. Mogilner, *Cell division*, Nature **422**(6933), 746 (2003).

[17] I. A. Berlatzky, A. Rouvinski and S. Ben-Yehuda, *Spatial organization of a replicating bacterial chromosome*, Proceedings of the National Academy of Sciences **105**(37), 14136 (2008).

[18] C. Butan, L. M. Hartnell, A. K. Fenton, D. Bliss, R. E. Sockett, S. Subramaniam and J. L. Milne, *Spiral architecture of the nucleoid in bdellovibrio bacteriovorus*, Journal of bacteriology **193**(6), 1341 (2011).

[19] D. Chaudhuri and B. M. Mulder, *Spontaneous helicity of a polymer with side loops confined to a cylinder*, Physical review letters **108**(26), 268305 (2012).

[20] R. Chelakkot, A. Gopinath, L. Mahadevan and M. F. Hagan, *Flagellar dynamics of a connected chain of active, polar, brownian particles*, Journal of The Royal Society Interface **11**(92), 20130884 (2014).

[21] A. Ghosh and N. Gov, *Dynamics of active semiflexible polymers*, Biophysical journal **107**(5), 1065 (2014).

[22] S. K. Anand, R. Chelakkot and S. P. Singh, *Beating to rotational transition of a clamped active ribbon-like filament*, Soft matter **15**(39), 7926 (2019).

[23] R. E. Isele-Holder, J. Elgeti and G. Gompper, *Self-propelled worm-like filaments: spontaneous spiral formation, structure, and dynamics*, Soft matter **11**(36), 7181 (2015).

[24] H. Vandebroek and C. Vanderzande, *Dynamics of a polymer in an active and viscoelastic bath*, Physical Review E **92**(6), 060601 (2015).

[25] B. Biswas, R. K. Manna, A. Laskar, P. S. Kumar, R. Adhikari and G. Kumaraswamy, *Linking catalyst-coated isotropic colloids into "active" flexible chains enhances their diffusivity*, ACS nano **11**(10), 10025 (2017).

[26] A. Ravichandran, G. A. Vliegenthart, G. Saggiorato, T. Auth and G. Gompper, *Enhanced dynamics of confined cytoskeletal filaments driven by asymmetric motors*, Biophysical journal **113**(5), 1121 (2017).

[27] A. Laskar and R. Adhikari, *Filament actuation by an active colloid at low reynolds number*, New Journal of Physics **19**(3), 033021 (2017).

[28] M. Abkenar, K. Marx, T. Auth and G. Gompper, *Collective behavior of penetrable self-propelled rods in two dimensions*, Physical Review E **88**(6), 062314 (2013).

[29] K. Prathyusha, S. Henkes and R. Sknepnek, *Dynamically generated patterns in dense suspensions of active filaments*, Physical Review E **97**(2), 022606 (2018).

[30] N. Gupta, A. Chaudhuri and D. Chaudhuri, *Morphological and dynamical properties of semiflexible filaments driven by molecular motors*, Physical Review E **99**(4), 042405 (2019).

[31] S. K. Anand and S. P. Singh, *Behavior of active filaments near solid-boundary under linear shear flow*, Soft Matter **15**(19), 4008 (2019).

[32] A. Kaiser, S. Babel, B. ten Hagen, C. von Ferber and H. Löwen, *How does a flexible chain of active particles swell?*, The Journal of chemical physics **142**(12) (2015).

[33] S. Das, N. Kennedy and A. Cacciuto, *The coil–globule transition in self-avoiding active polymers*, Soft Matter **17**(1), 160 (2021).

[34] A. Panda, R. G. Winkler and S. P. Singh, *Characteristic features of self-avoiding active brownian polymers under linear shear flow*, Soft Matter **19**(44), 8577 (2023).

[35] A. Kaiser and H. Löwen, *Unusual swelling of a polymer in a bacterial bath*, The Journal of chemical physics **141**(4), 044903 (2014).

[36] T. Eisenstecken, G. Gompper and R. G. Winkler, *Conformational properties of active semiflexible polymers*, Polymers **8**(8), 304 (2016).

[37] R. G. Winkler and G. Gompper, *The physics of active polymers and filaments*, The Journal of Chemical Physics **153**(4), 040901 (2020).

[38] T. Eisenstecken, G. Gompper and R. G. Winkler, *Internal dynamics of semiflexible polymers with active noise*, The Journal of chemical physics **146**(15) (2017).

[39] A. Martín-Gómez, G. Gompper and R. Winkler, *Active brownian filamentous polymers under shear flow*, Polymers **10**(8), 837 (2018).

[40] N. Samanta and R. Chakrabarti, *Chain reconfiguration in active noise*, Journal of Physics A: Mathematical and Theoretical **49**(19), 195601 (2016).

[41] S. K. Anand and S. P. Singh, *Conformation and dynamics of a self-avoiding active flexible polymer*, Physical Review E **101**(3), 030501 (2020).

[42] S. Paul, S. Majumder and W. Janke, *Activity mediated globule to coil transition of a flexible polymer in a poor solvent*, Soft Matter **18**(34), 6392 (2022).

[43] V. Bianco, E. Locatelli and P. Malgaretti, *Globulelike conformation and enhanced diffusion of active polymers*, Physical review letters **121**(21), 217802 (2018).

[44] S. K. Anand and S. P. Singh, *Structure and dynamics of a self-propelled semiflexible filament*, Physical Review E **98**(4), 042501 (2018).

[45] C. A. Philipps, G. Gompper and R. G. Winkler, *Tangentially driven active polar linear polymers—an analytical study*, The Journal of Chemical Physics **157**(19) (2022).

[46] A. R. Tejedor, J. Ramírez and M. Ripoll, *Progressive polymer deformation induced by polar activity and the influence of inertia*, Phys. Rev. Res. **6**, L032002 (2024), doi:10.1103/PhysRevResearch.6.L032002.

[47] M. Fazelzadeh, E. Irani, Z. Mokhtari and S. Jabbari-Farouji, *Effects of inertia on conformation and dynamics of tangentially driven active filaments*, Physical Review E **108**(2), 024606 (2023).

[48] A. Zidovska, D. A. Weitz and T. J. Mitchison, *Micron-scale coherence in interphase chromatin dynamics*, Proc. Natl. Acad. Sci. USA **110**, 15555 (2013).

[49] J. Smrek and K. Kremer, *Small activity differences drive phase separation in active-passive polymer mixtures*, Phys. Rev. Lett. **118**, 098002 (2017), doi:10.1103/PhysRevLett.118.098002.

[50] D. Saintillan, M. J. Shelley and A. Zidovska, *Extensile motor activity drives coherent motions in a model of interphase chromatin*, Proc. Natl. Acad. Sci. USA **115**, 11442 (2018), doi:10.1073/pnas.1807073115.

[51] I. Tiwari, P. Parmananda and R. Chelakkot, *Periodic oscillations in a string of camphor infused disks*, Soft Matter **16**(45), 10334 (2020).

[52] R. Chelakkot, M. F. Hagan and A. Gopinath, *Synchronized oscillations, traveling waves, and jammed clusters induced by steric interactions in active filament arrays*, Soft matter **17**(4), 1091 (2021).

[53] J.-X. Li, S. Wu, L.-L. Hao, Q.-L. Lei and Y.-Q. Ma, *Nonequilibrium structural and dynamic behaviors of polar active polymer controlled by head activity*, Physical Review Research **5**(4), 043064 (2023).

[54] J. Louten, *Virus structure and classification*, Essential human virology p. 19 (2016).

[55] J. Miller, C. Zeng, N. S. Wingreen and C. Tang, *Emergence of highly designable protein-backbone conformations in an off-lattice model*, Proteins: Structure, Function, and Bioinformatics **47**(4), 506 (2002).

[56] B. Chakrabarti, Y. Liu, J. LaGrone, R. Cortez, L. Fauci, O. Du Roure, D. Saintillan and A. Lindner, *Flexible filaments buckle into helicoidal shapes in strong compressional flows*, Nature Physics **16**(6), 689 (2020).

[57] R. Chelakkot, R. G. Winkler and G. Gompper, *Flow-induced helical coiling of semiflexible polymers in structured microchannels*, Physical review letters **109**(17), 178101 (2012).

[58] A. Shee, N. Gupta, A. Chaudhuri and D. Chaudhuri, *A semiflexible polymer in a gliding assay: reentrant transition, role of turnover and activity*, Soft Matter **17**(8), 2120 (2021).

[59] Y. Fily, P. Subramanian, T. M. Schneider, R. Chelakkot and A. Gopinath, *Buckling instabilities and spatio-temporal dynamics of active elastic filaments*, Journal of the Royal Society Interface **17**(165), 20190794 (2020).

[60] S. A. Sabeur, F. Hamdache and F. Schmid, *Kinetically driven helix formation during the homopolymer collapse process*, Physical Review E—Statistical, Nonlinear, and Soft Matter Physics **77**(2), 020802 (2008).

[61] J. P. Kemp and J. Z. Chen, *Helical structures in proteins*, Biomacromolecules **2**(2), 389 (2001).

[62] B. Biswas, D. Mitra, F. Kp, S. Bhat, A. Chatterji and G. Kumaraswamy, *Rigidity dictates spontaneous helix formation of thermoresponsive colloidal chains in poor solvent*, ACS nano **15**(12), 19702 (2021).

[63] L. Giomi and L. Mahadevan, *Statistical mechanics of developable ribbons*, Physical review letters **104**(23), 238104 (2010).

[64] E. M. Purcell, *Life at low reynolds number*, In *Physics and our world: reissue of the proceedings of a symposium in honor of Victor F Weisskopf*, pp. 47–67. World Scientific (2014).